Available online at www.sciencedirect.com

ScienceDirect

Procedia Structural Integrity 43 (2023) 154–159

Structural Integrity Procedia

www.elsevier.com/locate/procedia

10th International Conference on Materials Structure and Micromechanics of Fracture

Quenching of Carbon Steel Plates with Water Impinging Jets: Differential Properties and Fractography

Pavel Romanov[a,b]*, Mohammad Jahedi[b], Anders Petersson[c], Bahram Moshfegh[b,d], Mattias Calmunger[a,b]

[a]*Division of Engineering Materials, Linköping University, 58183 Linköping, Sweden*
[b]*Division of Building, Energy and Environmental Engineering, University of Gävle, 80176 Gävle, Sweden*
[c]*Väderstad Components AB, 59472 Överum, Sweden*
[d]*Division of Energy Systems, Linköping University, 58183 Linköping, Sweden*

Abstract

The demand for steel components with tailored properties is constantly growing. To obtain a specific variation of microstructures and mechanical properties along the component it must undergo a controllable cooling. One way to control the cooling rates along the component is by using different simultaneous water jet impingements on a hot austenitized surface. This can be done by a newly developed test rig for water Impinging Jet Quenching Technique (IJQT). This work discusses the effect of IJQT on mechanical properties and fracture behavior of 15 mm steel plates containing 0.27 and 0.38 mass-% carbon. The samples were cooled in a specifically designed setup of the technique to obtain simultaneous water and air cooling resulting in diverse microstructures. The mechanical property gradients of both steels were analyzed through hardness measurements and tensile tests. The fracture surfaces and the near fracture regions were observed using scanning electron microscope and light optical microscope respectively.

The results from tensile tests showed that the larger part of the sample with higher carbon content was fully hardened, however smoothly transitioning to a more ductile region. The sample with lower carbon content combined various degrees of hardening and transitioned from higher to lower ultimate tensile strength values. Fracture behavior of higher carbon steel was predominantly brittle transitioning to a ductile, while the lower carbon steel had a small region showing brittle fracture transitioning to a larger region of predominant ductile fracture behavior.

Keywords: Martensite; Brittle fracture; Ductile fracture; Impinging Jet Quenching; Boron steel;

* Corresponding author. Tel.: +46-13-282537.
E-mail address: pavel.romanov@liu.se

2452-3216
10.1016/j.prostr.2022.12.251

1. Introduction

Accurately designed components with tailored mechanical properties are mandatory in many applications. Conventional immersion into quenching medium does not provide an accurate control of the local cooling rates along the part, therefore tailoring for example in automobile industry is done by tool quenching during hot stamping (Merklein et al. 2016) or by spray quenching (Ying et al. 2020).

These methods successfully work for relatively thin steel sheets, however, a mechanical property gradient may also be beneficial for much thicker steel plates used for agriculture machinery parts, such as discs, cultivating points or plowshares. These components in general need to have high wear resistance, high hardness and strength (Bhakat et al. 2007), therefore high cooling rates are required during quenching to obtain hard martensitic condition through the whole thickness, however, in order to differentiate the cooling, it has to be accurately controlled.

One way to obtain different continuous cooling rates and thus diverse microstructure gradient and mechanical properties is by using water jet impingements which has not been investigated with implementation on thick plates. Therefore, the aim of this study is, by using Impinging Jet Quenching Technique (IJQT), to harden 15 mm thick steel plates to a varying hardening degree along their lengths, and to analyze the effect of such differential cooling on mechanical properties and types of fracture of 0.27 and 0.38 wt% C steels. The results will contribute to a further optimization and development of the IJQT for a more advanced heat-treating route of thick steel components.

The test rig for IJQT consists of a test chamber and induction heater and has working principle as following: First, the steel test sample is assembled to the holder inside the test chamber and the induction heater heats the sample to a desired austenitization temperature. The heater is then replaced by a nozzle pattern through which water is supplied at a certain jet speed and quenches the component. For a detailed description of the test rig, the reader is referred to the work of Jahedi (2021).

2. Quenching Experiments

2.1. Experimental Setup

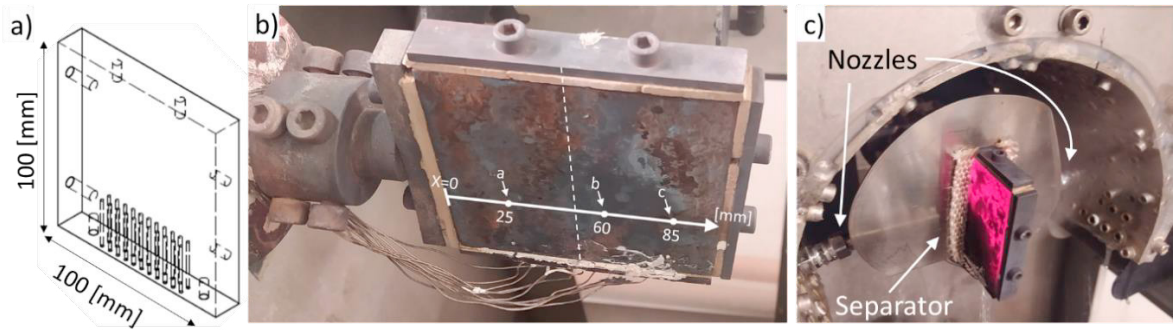

Fig. 1. a) 3D view of the test sample; b) test sample attached to a holder inside the test chamber; c) austenitized test sample undergoes quenching.

A drawing of a 15 mm thick carbon steel sample is shown in Fig. 1.a) which contains 22 narrow holes for the thermocouples. This sample was attached to a holder inside the test chamber as shown in Fig. 1.b), and N-type thermocouples were embedded into the holes and covered with a special cement on the outer side for insulation. The sample was then austenitized for 12 minutes at 915 °C. After that the heater was replaced by a manually designed nozzle pattern surrounding the red austenitized sample as shown in Fig. 1.c). The water is supplied through the two nozzles of 8 mm in diameter located one on each side of the sample to obtain a symmetrical quenching. A separator was also tightly attached at the middle of the sample with the purpose to isolate the right part of the sample from direct contact with water. In this way the left side of the sample undergoes a faster cooling due to impingement of the water jets, and the right side undergoes slower cooling by heat transfer inside the sample and by natural convection in air. Fig. 1.c) shows the differential quenching process where the sample combines red and black colors due to temperature differences at that specific time during the quenching experiment. All further analysis in this study is performed at the depth of 7.5 mm inside the sample and along its length as indicated with a measurement line in Fig. 1.b).

2.2. Materials and Methods

Two types of carbon steels containing boron were tested in the experimental setup. Boron steel is widely used for example in automobile industry and for agriculture machinery parts due to its high hardenability which is achieved by small addition of boron. Table 1 shows the nominal chemical composition of the steels: Boron 27 (B27) and Boron 38 (B38) where the number in their designations is referred to their carbon content.

Table 1. Nominal chemical composition of the steels (in mass-%) obtained from the manufacturer.

Steel type designation	C	Si	Mn	S	P	Cr	B
Boron 27 (B27)	0.24 - 0.30	0.10 - 0.40	1.00 - 1.40	0.010	0.020	0.10 - 0.40	0.0008 -0.0050
Boron 38 (B38)	0.36 - 0.42	0.10 - 0.30	1.20 - 1.45	0.010	0.020	0.10 - 0.40	0.0008 -0.0050

After the quenching experiments, the samples were cut into smaller cubes and into 2 mm thick sheets using electrical discharge machining (EDM) as indicated with red solid lines in Fig. 2.a). Small cubes were used for hardness measurements and the thin sheets were afterwards cut into miniature tensile specimens shown in Fig. 2.b).

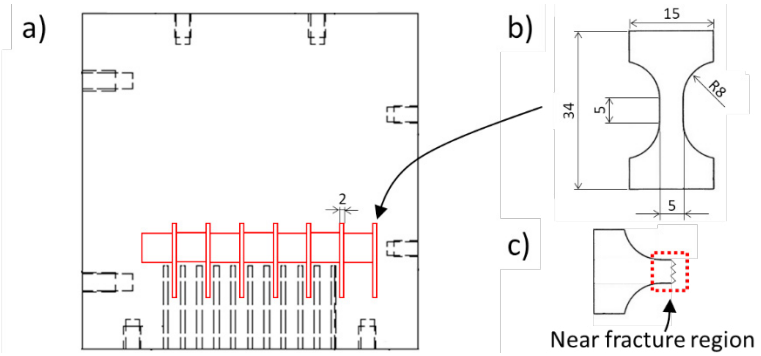

Fig. 2. a) test sample; b) tensile specimen (thickness is 2 mm); c) near fracture region for observation with microscope

The samples were mounted in Struers PolyFast and polished with 3, 1 and 0.25 µm diamond suspensions using Struers Tegramin-30 polishing machine. 3% Nital etchant was used to reveal the microstructure which was observed with Leica DM6 M light optical microscope equipped with the Leica LAS X software. Hardness measurements were performed according to ASTM E384 standard, with a 5 kgf load, using a Struers DuraScan 70 G5 hardness tester with a Vickers diamond equipped. Tensile tests were performed with a 10^{-3} s^{-1} strain rate and 50 Hz logging frequency using Alwetron TCT50 machine equipped with 100 kN load cell and Inersjö CyclicEdc application software. The near fracture region was cut from the tested tensile specimen, as shown in Fig. 2.c) with red dashed line, and metallurgically prepared in the same way as described. Hitachi SU-70 field emission SEM at 10 kV acceleration voltage with 7 mm working distance was used for observations of the cracks and fracture surfaces of the tested tensile specimens.

3. Results and Discussion

3.1. Mechanical Properties

Due to the difference in chemical compositions, the hardness and ultimate tensile strength (UTS) profiles of both steels demonstrate different behavior which can be seen in Fig. 3. B38 shows high and more or less constant UTS and hardness values at the distance of up to 50 mm. The UTS of 2000-2100 MPa at this distance corresponds to a fully hardened condition, as reported by Taylor et al. (2014) in the study of a similar steel. Further along the sample the hardness starts to deviate, and strength starts to decrease. This hardness and strength behavior along the B38 sample indicates a smooth transition from a higher to lower hardening degree.

B27 shows lower hardness and UTS than B38 in general, which is expected due to its lower carbon content, and also shows a similar trend of decrease. However, the highest UTS values of 1500 MPa are located at the distance of

up to 35 mm. Further the properties gradually decrease between 35 and 70 mm and the strength stabilize afterwards at around 700-800 MPa. According to Frydman and Letkowska (2012), a fully hardened and a normalized condition of B27 should provide a TS of 1762 and 598 MPa respectively. This variation of strength along the B27 sample also indicates a smooth transition from a higher to a lower hardening degree.

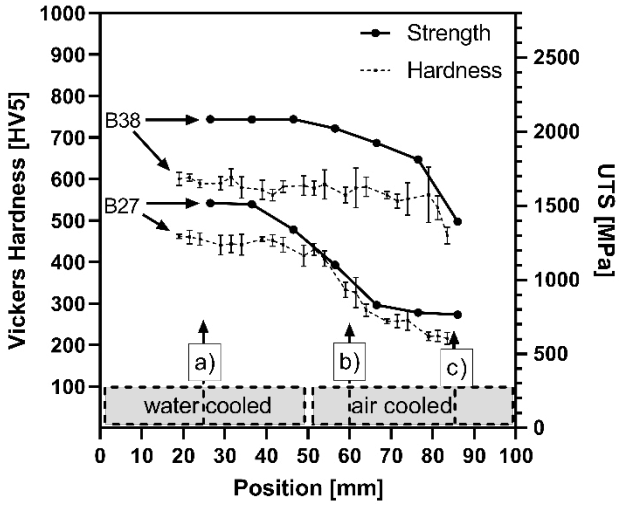

Fig. 3. UTS and hardness profiles of B27 and B38 samples (x-axis is the position on the measurement line in Fig. 1.b).

3.2. Fracture Surfaces

In order to analyze and compare the most, the medium and the least hardened conditions, which B27 and B38 samples have acquired from heat treatment with IJQT, the fracture surfaces of the tensile specimens were observed at the positions: 25, 60 and 85 mm (indicated a), b) and c) in Fig. 3). The SEM pictures of the fracture surfaces of B38 are shown in Fig. 4.

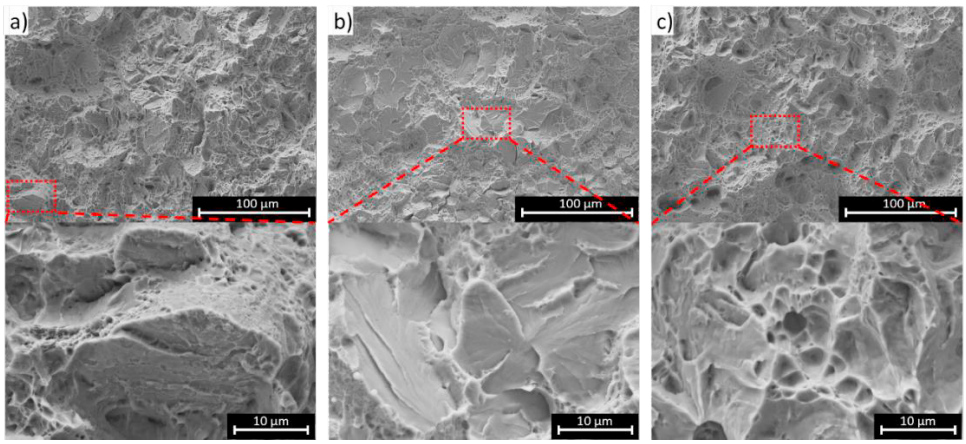

Fig. 4. Fracture surfaces of B38 sample at positions: a) 25 mm; b) 60 mm; c) 85 mm.

From Fig. 4.a) and Fig. 4.b), which correspond to 2100 MPa and 2000 MPa UTS respectively (see Fig. 3), it is seen that the fractures predominantly had a brittle behaviour due to relatively flat surfaces, sharp edges and absence of dimples. This also provides an extra confirmation for a fully hardened condition which is expected to be brittle due to martensite. In Fig. 4.c), which correspond to 1400 MPa, the surface looks the same at first glance, however at a higher magnification the dimples are clearly visible and indicate a ductile fracture.

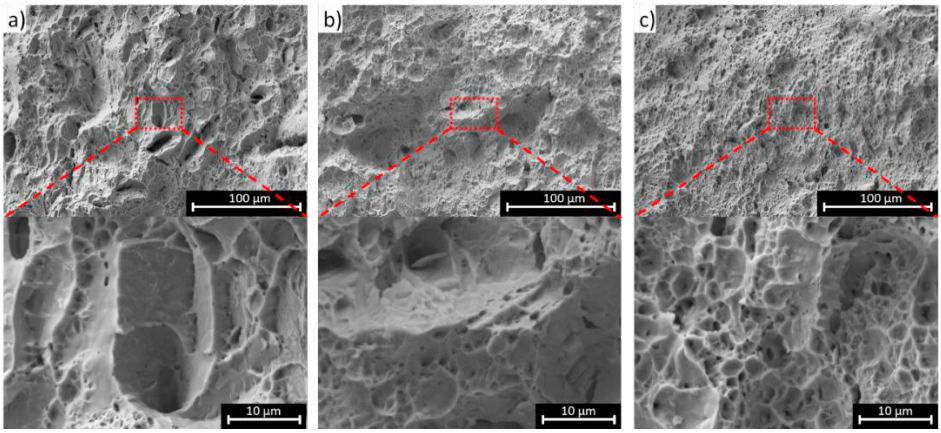

Fig. 5. Fracture surfaces of B27 sample at positions: a) 25 mm; b) 60 mm; c) 85 mm.

The surface of B27 tensile specimen at 25 mm, which corresponds to 1500 MPa UTS, shows predominantly brittle fracture due to sharp facets, however dimples are also observed indicating a mix of both brittle and ductile fractures. In Fig. 5.b) one may find a trace of sharp edges that are covered with dimples, and in Fig. 5.c) no features of brittle fracture are observed. The fact that all fracture surfaces of B27 showed more or less ductile type of fracture provides extra confirmation for the hardening profile of B27, specifically that a fully hardened region is absent.

3.3. Near Fracture Region

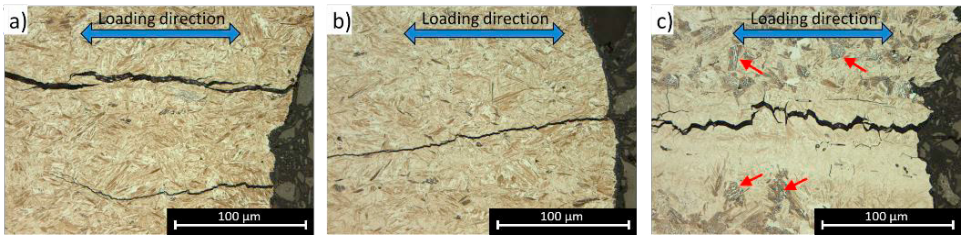

Fig. 6. Near fracture regions of B38 sample at positions: a) 25 mm; b) 60 mm; c) 85 mm.

B38 sample consists of lath martensite at 25 and 60 mm, as seen in Fig. 6.a) and b). At 85 mm the microstructure consists of martensite and some lamellar structure of bainite or pearlite (red arrows). This explains the decrease in hardness and strength at this distance interval. Another thing worth noticing is that all three observed near fracture regions contain one or more cracks perpendicular to the main fracture and parallel to the loading direction (blue arrows). At 25 and 60 mm these cracks propagate through martensite and are unremarkable, however at 85 mm it is clearly seen that the crack propagates through a brighter region of the microstructure similar to martensite while the regions above and beyond clearly contain lamellar structures of bainite or pearlite (red arrows). One explanation to this can be the defects from initial manufacturing with hot rolling and insufficient austenitization which in this experiment was performed in the same way for both types of steel.

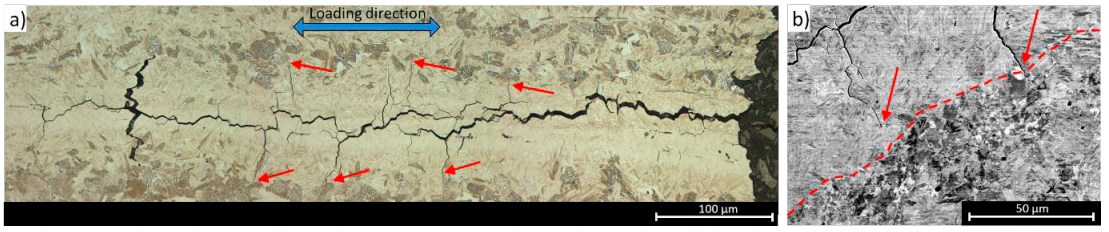

Fig. 7. Near fracture regions of B38 tensile specimen at 85 mm: a) picture of a crack parallel to the tensile loading; b) perpendicular secondary cracks observed with SEM.

The crack from Fig. 6.c) was studied further and shown in Fig. 7.a) with perpendicular branching cracks (red arrows). It is clearly seen that the branching cracks propagate vertically i.e., perpendicular to the loading direction and clearly stops when reaching the lamellar structure. The region where the branching cracks abrupt was observed with SEM using BSE detector (Fig. 7.b) and it is clearly visible that the cracks (marked with red arrows) stop where the microstructure becomes more deformed, which is sectioned with red dashed line.

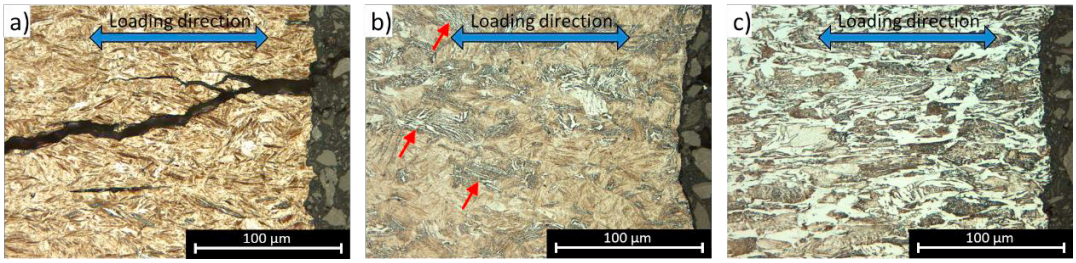

Fig. 8. Near fracture regions of B27 sample at positions: a) 25 mm; b) 60 mm; c) 85 mm.

B27 sample at 25 mm also contains predominantly martensite as seen in Fig. 8.a), however some rare regions of ferrite were also observed. At 60 mm the microstructure contains both martensite and lamellar structures of ferrite or bainite (red arrows in Fig. 8.b). At 85 mm the elongated grains of ferrite and pearlite are clearly visible (Fig. 8.c). A crack parallel to the loading direction is only occurred at 20 mm and not at 60 mm or 85 mm. Explanation for that may be a higher ductility and a lower UTS at these corresponding regions as shown in Fig. 3.

4. Conclusions

Both B27 and B38 samples were successfully hardened using IJQT to various degrees providing different levels of hardness and UTS along 15 mm thick boron steel components, specifically: B38 sample acquired after heat treatment a fully hardened region, that smoothly transitions to a more ductile region. Larger part of the B38 sample had predominantly brittle fractures during tensile tests. B27 sample acquired after heat treatment a whole range of hardening degrees and the fractures were predominantly ductile. Proper and accurate austenitization are important for eliminating the consequences from initial manufacturing process, which can affect the mechanical properties and behavior of the steel during fracture. Further study is focused on a more detailed characterizations and simulations of the microstructure evolutions during differential cooling experiments with IJQT.

Acknowledgements

The present study was financed by Sweden's Innovation Agency Vinnova (2017-02281) and by the Swedish Agency for Economic and Regional Growth (20201438).

References

Bhakat, A.K., A.K. Mishra, and N.S. Mishra. 2007. "Characterization of Wear and Metallurgical Properties for Development of Agricultural Grade Steel Suitable in Specific Soil Conditions." *Wear* 263(1–6): 228–33.

Frydman, S., and B. Letkowska. 2012. "Properties of Boron Steel after Different Heat Treatments." *MTM Machine, Technol., Mater 6* (9): 44–46.

Jahedi, Mohammad. 2021. "Experimental and Numerical Investigation of the Quenching Process on Rotary Hollow Cylinder by Multiple Impinging Jets." University of Gävle.

Merklein, Marion et al. 2016. "Hot Stamping of Boron Steel Sheets with Tailored Properties: A Review." *Journal of Materials Processing Technology* 228: 11–24. http://dx.doi.org/10.1016/j.jmatprotec.2015.09.023.

Taylor, T., G. Fourlaris, P. Evans, and G. Bright. 2014. "New Generation Ultrahigh Strength Boron Steel for Automotive Hot Stamping Technologies." *Materials Science and Technology* 30(7): 818–26.

Ying, Liang et al. 2020. "Experimental and Numerical Investigation on Temperature Field and Tailored Mechanical Properties Distribution of 22MnB5 Steel in Spray Quenching Process." *Journal of Manufacturing Processes* 57: 930–56.